10 Measuring techniques

Since human beings do not possess any sense for the detection of ionizing radiation, they must entirely rely on special instruments in order to prevent or control any harmful radiation exposure or intake of radioactivity from the outset. Therefore, reliable instruments and methods for radiation detection and measurement form the precondition for the safe handling of radiation and radioactivity in medicine, scientific research, industry, and nuclear energy production. As summarized in Table 10.1, the primary tasks of radiation protection measurements can roughly be divided into dose and activity measurements employed to prevent and control hazard to man from ionizing radiation (external exposure) or the incorporation of radioactivity (internal exposure), respectively. The purpose of this Chapter is to give a short overview of radiation detectors frequently utilized for these tasks (10.1) and of their application in practice to monitor and quantify external (10.2) and internal exposures (10.3).

10.1 Detectors for radiation protection

10.1.1 Overview and general characteristics of radiation detectors

The function of a detector designed of measuring ionizing radiation is to generate a measurable response that is related to the energy deposited in the detector material or the number of particles entering into it – such as the charge produced in a gas, the intensity of visible light emitted by some solid or liquid matter, the degree of blackening of a photographic film, or the number of chromosome aberrations in a biological sample. The most common radiation effects used for radiation protection measurements are summarized in Table 10.2. In this Chapter (10.1) the emphasis is on how these detectors – and the instruments based on them – respond to radiation and how this response can be interpreted to determine the desired quantity such as dose, exposure, or activity. Clearly, radiation protection measurements are performed by means of instruments common to other fields of radiation detection and measurement (e.g. nuclear and particle physics, radiation therapy, diagnostic radiology, and nuclear medicine). Therefore, much has been published about the design and operation of these devices. An enormous amount of information is provided, among others, in the excellent textbooks by Attix [86Att], Kiefer and Maushart [72Kie], Knoll [00Kno], Leo [94Leo], Lutz [99Lut], Shani [00Sha], Tsoulfanides [95Tso], and in the comprehensive three-volume treatise edited by Attix, Roesch, and Tochilin [68Att]. These texts form the basis of the following brief review and the reader is referred to them for supplementary information and an exhaustive bibliography.

Table 10.1. Major objectives and categorization of radiation protection measurements.

Objective of Measurement	External exposure	Internal exposure
Prevention of exposure	Area monitoring Assessment of protective measures	Determination and identification of radioactivity in air, water, and food that may be incorporated Environmental monitoring Detection of surface or skin contaminations
Control of Exposure	Personal monitoring	Determination and identification of incorporated radioactivity by in vivo and excretition measurements

Table 10.2. Radiation effects frequently used for radiation protection measurements (adapted from [96Hoh]).

Radiation effect	Type of instrument	Detector material	Determination of dose or dose rate	Determination of activity or particle counting	Identification of radionuclides
Electrical	Ionization chamber	Gas	++	+	+
	Proportional counter	Gas	+	++	++
	Geiger-Müller counter	Gas	+	++	
	Semiconductor detector	Crystalline semiconductor	++	++	++
Optical	Scintillation counter	Crystal, plastic, or liquid	++	++	++
	Thermoluminescence dosimeter	Crystal	++		
	Radiophotolumines-cence dosimeter	Glas	+		
Thermal	Superheated drop detector	Liquid drops	+		
Chemical	Film	Photographic emulsion	++		
	Etched-track detector	Plastic foil	+		
Biological	Scoring of chromo-somal aberrations	Chromosomes	+		

++ : frequently employed, recommended procedure
+ : in specific cases usefully applicable

Before the different radiation detectors mentioned in Table 10.2 are described in more detail in the sub-sequent Sections, two fundamental aspects which are relevant for all of them are outlined [68Att, 86Att]:

Absolute measurement and calibration. A device is regarded as ‘absolute’ if it can be constructed and subsequently used to measure radiation without the necessity of calibrating its response in a known radiation field. Such instruments are primarily installed and operated in national standards laboratories. For radiation protection measurements it is sufficient to use devices that are properly calibrated by accredited laboratories that guarantee traceability to an official standards laboratory. Calibration can be accomplished, for example, by exposing a device (in some cases in or in front of an appropriate phantom) in a reference radiation field, and then determining a calibration factor N by which the detector reading R has

to be multiplied to achieve the true value of the measurand. If the quantity to be measured is not linearly related with detector response, a calibration curve has to be established by varying the considered parameter of the radiation field over the relevant range. It is important to note, that detector response generally depends on the type and energy of the radiation (photons or particles) to be detected. Due to this reason, calibration of a radiation measuring instrument is restricted to a specified range of both the quantity to be determined and the energy of the radiation considered.

Repeatability, accuracy, and uncertainty. The repeatability of an instrument is its ability to yield the same result for repeated measurements in a constant radiation field. Consequently, it can be stated in terms of the standard deviation estimated from the readings of repeated measurements. On the other hand, the accuracy of an instrument expresses the closeness of the reading to the true value of the quantity being measured and, thus, mainly depends on the correctness of its calibration. In other words: repeatability characterizes random errors due to instabilities of the instrument and the stochastic character of ionizing radiation, whereas accuracy quantifies systematic errors of the measurement process. In general, the result of a measurement is only an approximation of the true value of the measurand, and thus is complete only when accompanied by a quantitative statement of its uncertainty, i.e. an interval within which the true value lies with given probability [95ISO]. Possible sources of error in radiation dosimetry and procedures for estimating the resulting magnitude of the uncertainties in the measurement results can be found in [02ISO].

10.1.2 Gas-filled ionization detectors

10.1.2.1 Ionization and gas amplification

Ionization detectors were the first electrical devices developed for radiation detection. They are still widely used for radiation protection measurements. Radiation detection is based on the collection of electrons and ions produced by ionizing particles in the detector material – preferential a gas because of the high mobility of electrons and ions in this medium. An atom can be ionized in a variety of ways, but collisions of charged particles with the atomic electrons via Coulomb interaction are the most important mechnisms. For most gases of practical interest, the average energy W spent by a charged particle to produce an electron-ion pair is between 20 and 40 eV [79ICR]. In air, for example, the value is about 36 and 34 eV for α and β particles, respectively. Consequently, a charged particle will produce a large number of electron-ion pairs if it deposits its energy completely in the gas.

As shown in Fig. 10.1, a typical detector configuration consists of an anode wire inside of a cylindrical cathode. When an electric potential difference (voltage) is applied between the electrodes, electrons and ions are attracted to the electrodes and generate an electric output signal, which is passed through a series of electronic circuits for amplification, processing, and storage. There are two different ways to process the signal. In the pulse mode, the electrical signal from each event is processed individually, whereas in the current mode, the signals from individual interactions are integrated, yielding a net current signal. Depending on the voltage between the electrodes, there are three basic types of gas-filled ionization detectors taking advantage of different physical effects: the ionization chamber, the proportional chamber, and the Geiger-Müller counter. To understand the differences between these devices, consider – under the assumption of a constant flux of radiation – the behavior of a gas-filled ionization detector as the electrical voltage is increased. As illustrated in Fig. 10.2 for two different types of particles, six different regions of operation can be distinguished [00Kno, 94Leo]:

At very low voltages, the electric field is insufficient to avoid recombination of the electron-ion pairs. However, recombination is lessened as the voltage is raised, giving rise to a saturation curve (region I). Usually, the saturation curve reaches a more or less distinct plateau, where the number of ions collected is nearly independent of the applied voltage. A detector operating in this region (II) is denoted as *ionization chamber*.

As the voltage across the device is raised further, the number of ions collected starts to increase again, because the electric field is strong enough to accelerate electrons from the primary ionization to kinetic energies that are sufficiently high to ionize further gas molecules by collisions (secondary ionization). In the case of a cylindrical detector arrangement, the electrical field increases steeply near the anode wire and thus the amplification process results in an electron 'avalanche' confined to a very small length of the anode wire. Due to this reason, electron avalanches initiated by primary ionizations at different points in the gas do not interfere and thus the output of the device is – for a given voltage – directly proportional to the number of primary ionizations or, equivalently, to the energy dissipated inside the detector volume. A detector operating in this region (III) is known as a *proportional counter*. Increasing the applied voltage still more results in a nonlinear amplification process (region IV) since the gain is so large that space-charge effects become relevant distorting the electrical field within the detector.

If the voltage between the electrodes exceeds the region of limited proportionality, the number of ions collected becomes independent of the type and energy of the incident particles. The reason is that instead of various independent avalanches confined to small Sections along the wire (as in regions III and IV), a chain reaction of many avalanches is triggered, which spread out along the entire wire. This transitory electrical breakdown is initiated by excited gas atoms undergoing radiative de-excitation. Ultraviolet photons emitted by these processes propagate to other parts of the gas volume and initiate secondary avalanches. Detectors working in this region (V) are called *Geiger-Müller counters*. As the voltage is further increased, a continuous breakdown occurs (region VI).

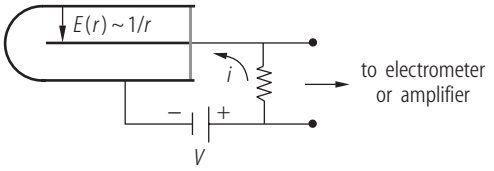

Fig. 10.1 Typical arrangement of a cylindrical ionization detector operated in the current mode. (*r*, radial distance from the anode wire; *E*, transaxial electric field strength).

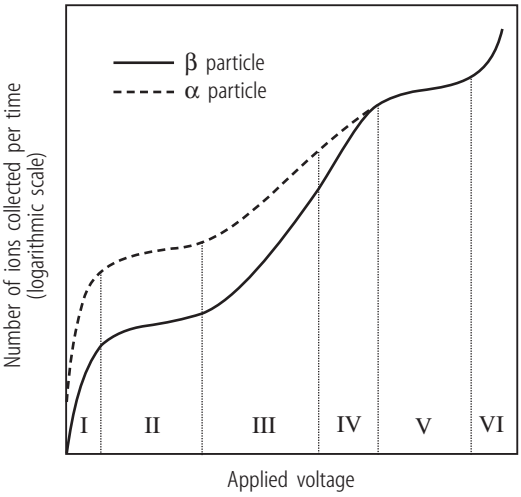

Fig. 10.2 Schematic plot showing the relation between the voltage applied to a gas-filled ionization detector and the charge collected for two different types of particles depositing different amounts of energy within the ion-collecting gas volume. Six regions of operation can be distinguished: I, recombination region; II, ionization region; III, proportional region; IV, limited proportional region; V, Geiger-Müller region; VI, discharge region.

10.1.2.2 Ionization chambers

Ionization chambers are frequently used for radiation protection measurements and are available in a large variety of types. They are normally used in the current and not in the pulse mode. The electrical current caused by a device operating in the ionization region, however, is much too small to be measured using conventional galvanometer techniques. Therefore, a sensitive electrometer with a sufficiently high impedance indirectly measures the electrical current in the circuit by detecting the voltage drop across a high-load series resistor (cf. Fig. 10.1 and [00Kno]). Depending on whether the charge or the current is measured, the chamber will register the total ionization that has occurred in a given time (exposure, dose) or the rate of ionization at any instant (exposure rate, dose rate).

To discuss the basic concepts, we first consider *free-air ionization chambers*, which are in operation primarily in national standards laboratories. They form the standard against which simpler instruments are compared to yield reliable calibration factors. A typical configuration of a parallel-plate ionization chamber is shown in Fig. 10.3. An important feature of this device is that the sensitive volume, i.e. the volume common to both the collecting volume defined by the electrical field between the plates and the collimated beam (cf. Fig. 10.3), is defined electronically and not by the walls of the chamber. Free-air chambers are specifically well-suited for the measurement of radiation exposure since this quantity – according to the operational definition given in Section 4.4.2.3 – is directly related to the ionization produced by collision interactions in air by charged particles resulting from interactions of photons (or neutrons). However, exposure measurements require the detection of all the ionization produced in the selecting volume. To this end, the lateral distance between each of the electrodes and the border of the sensitive volume must exceed the range of the secondary electrons which originate in the sensitive volume. This guarantees that electrons, the path of which remains within the collecting volume (like e_1 in Fig. 10.3), can produce all their ionization in this region where it will be collected and measured. But most electrons released in the sensitive volume will leave the collecting volume (like e_2) and thus part of the ionization they produce will not reach the collector. This loss, however, is of no relevance if as many electrons from photon interactions elsewhere in the beam enter the sensitive volume with the same energy (like e_3) as leave it. A detailed discussion of this condition, which is known as *charged particle equilibrium* (or in the considered case of a photon beam as *electronic equilibrium*), can be found in [86Att]. Charged particle equilibrium in the sensitive volume is attained when the photon flux remains constant across the chamber and when the distance from the diaphragm of the chamber to the border of the sensitive volume is greater than the maximum electron range. Since the maximum range of electrons in air increases rapidly with the energy of incident X- or γ-rays, the size of a free-air ionization chamber that can be realized in practice limits the energy of photons to be measured to about 200 keV.

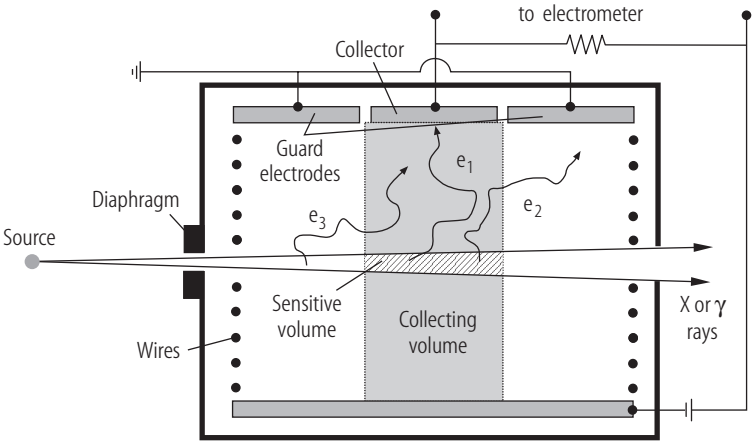

Fig. 10.3 Typical configuration of a parallel-plate free-air ionization chamber. The grounded guard electrodes and the electrically biased wires are used to produce a uniform electrical field within the collecting volume. The ionization measured is that produced by electrons in the collecting volume.

To avoid the use of large and cumbersome free-air ionization chambers, practical *cavity ionization chambers* have been developed which basically consist of a solid wall surrounding a gas-filled cavity. In this cavity an electric field is established to collect the ions produced by radiation entering the chamber (cf. Fig. 10.1). The criteria that determine the dimension and the material of a chamber depend on both the desired dosimetric quantity (exposure or absorbed dose) and the type and energy of the radiation to be measured. Cavity ionization chambers can be designed and operated either as equilibrium or Bragg-Gray chambers in which the local photon (or neutron) field or the local secondary charged-particle field is sufficiently well characterized, respectively [86Att].

Dosimetric measurements in photon and neutron fields can be performed with cavity chambers operated under *charged particle equilibrium* conditions. The physical basis is described by the Fano theorem which states that in an infinite medium of given atomic composition exposed to a uniform field of indirectly ionizing radiation, the field of secondary radiation is also uniform and independent of the density of the medium as well as of density variations from point to point [86Att]. That means that the ionization

collected in the gas is not influenced by the density of the wall, provided that the materials of the wall and the gas are matched with regard to their atomic composition – i.e. the effective atomic number Z – and that the thickness of the wall exceeds the range of the charged secondary particles released in the wall. The dimensions of the gas-filled cavity can be adapted to the flux of the radiation field to be measured in order to generate a sufficiently high ionization. For exposure measurements, the wall should be made of air-equivalent material with an effective atomic number of air, such as some plastics or graphite with silicon additives. Although there is no material that is exactly air-equivalent, the deviations are of minor importance for the purposes of radiation protection measurements. The use of cavity chambers operated under charged particle equilibrium conditions is limited to photons with an energy of less than about 3 MeV. At higher energies it is not possible to build a chamber that meets the two central conditions, namely a sufficiently thick wall to establish electronic equilibrium and negligible attenuation of the photon beam crossing the chamber. Chambers can also be made tissue-equivalent, which means that the atomic composition of both the wall and the gas must be similar to that of tissue. Since the absorbed dose in air or tissue (at a depth corresponding to the wall thickness) is directly proportional to the ionization per unit volume of gas measured under charged particle equilibrium conditions with an air- or tissue-equivalent chamber, respectively, these devices can be calibrated to directly read the desired dosimetric quantity.

Dosimetric measurements can also be performed with cavity ionization chambers taking advantage of the *Bragg-Gray principle*, which states that the absorbed Dose D_m in a given homogeneous medium can be calculated from the ionization produced in a small gas-filled cavity suspended into this material according to the equation $D_m = WS_{m-g}J$, where W is the average energy dissipated in the gas per electron-ion pair formed, S_{m-g} the ratio of the average mass stopping powers of the medium and the gas for the charged particles considered, and J the ionization per unit volume of gas. This principle holds under two conditions: Firstly, the cavity must be small compared to the range of the charged particles striking so that the flux and energy spectrum of the charged particles is not disturbed. Secondly the energy lost by the charged particles in crossing the gas-filled cavity is equal to the energy deposited in the gas volume [86Att]. In practice, the gas-filled cavity is part of a cavity chamber with a wall that separates the cavity from the surrounding material. Therefore, the chamber wall should be either extremely thin to leave the charged particle field unchanged or matched to the atomic composition of the surrounding medium. Bragg-Gray cavity chambers can be used for dosimetry of charged particles, entering from outside the chamber, and of high-energy photons (>3 MeV) liberating electrons in the chamber wall.

In practice, neither the idealized conditions of charged particle equilibrium nor that of the Bragg-Gray principle can be fully realized and thus a variety of corrections must be applied in order to make absolute dosimetric measurements possible. For radiation protection measurements, however, this complex task can be avoided when chambers are used that are calibrated under conditions similar to those in which the instrument will be applied and in terms of the desired dosimetric quantity (e.g., exposure, absorbed dose, ambient dose equivalent, or the corresponding dose rates). As an example, Fig. 10.4 shows a portable survey instrument with an air-equivalent chamber that can be used for dose and dose rate measurements over a wide range of photon energies.

Fig. 10.4 Dose and dose rate survey meter with an air- equivalent ionization chamber (volume 600 cm^3) for the measurement of X- and γ-rays in the energy range between 6 keV and 3 MeV. Using an additional plastic shielding, even photons up to an energy of 7.5 MeV can be measured. The probe is detachable for remote measurements. (Courtesy Step Sensortechnik).

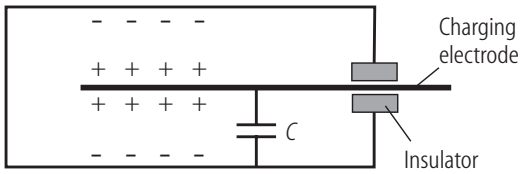

Fig. 10.5. Schematic representation of a condenser-type ionization chamber.

Other types of portable ion chambers are based on the charge integration principle illustrated in Fig. 10.5. In this case, the chamber electrodes are connected in parallel with a capacitor, which is initially charged up to establish an electric field in the chamber. When the chamber is exposed to radiation, the ionization caused in the gas-filled chamber is collected by the electrodes and the charge stored in the capacitor is reduced. The resulting drop in chamber voltage can be used as a measure of the total integrated ionization charge. In the case of a self-reading '*pocket dosimeter*' employed for personal radiation protection measurements, a simple rugged quartz-fiber is mounted inside the ionization volume which is deflected when the device is charged. The position of the fiber, which varies as the charge on the capacitor is reduced due to ionizing radiation, is observed through a small built-in microscope that has a scale in the eyepiece (Fig. 10.6). The position against the scale can be calibrated in terms of the total radiation recorded by the pocket dosimeter. Over a longer period of time, however, leakage currents across the insulator surface can not be avoided and this limits the accuracy of the dosimeter.

Progress in integrated circuit technology resulted in the development of *direct ion storage (DIS) dosimeters*, which combine a gas-filled ionization chamber with a non-volatile electronic charge storage element [96Kah, 00Kno, 99Wer]. A schematic representation of a DIS dosimeter is shown in Fig. 10.7. The charge is initially placed on the floating gate of a standard EEPROM (electrically erasable and programmable read-only memory) cell by injecting electrons by a tunneling process through the silicon oxide. Electrons are trapped at this gate for many years since at normal operating temperatures they have no conductive discharge path when the silicon dioxide formation is made of high-purity material (cf. Section 10.1.4). When the chamber is exposed to ionizing radiation, the ions produced in the fill gas are collected by the charged floating gate, which results in a reduction of the charge stored. Assessment of this quantity can be performed without changing the charge distribution by measuring the channel conductivity of the field effect transistor (FET), which forms the basis of the EEPROM, by means of an electronic readout unit. The passive electronic dosimeter thus makes it possible to instantly and non-destructively readout the accumulated dose whenever required. The first commercial DIS personal dosimeter consist of a series of separate dosimeter elements housed inside a small hermetically sealed container. Three elements are used for the measurement of the personal dose equivalent $H_p(10)$ in the range from 1 μSv to 40 Sv and two elements for the determination of $H_p(0.07)$ in the range between 10 μSv and 40 Sv [99Wer] (the definition of $H_p(d)$ is given in Section 4.5.3.4). The dose-rate linearity is flat up to 40 Sv/h thus guaranteeing accurate dose assessment in accident situations.

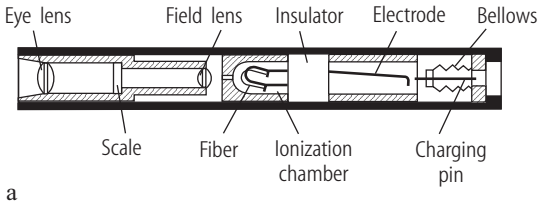

a

b

Fig. 10.6. Pen-size direct-reading ion chamber dosimeter for personal radiation protection measurements in a γ- or X-ray environment. **(a)** Simplified schematic representation. **(b)** Pocket dosimeters for different dose and energy ranges. The nominal voltage required to 'set the dosimeter to zero' is adjusted with the charging unit (potentiometer). A test source is used to check the correct function and calibration of the personal dosimeters. (Courtesy Thermo Eberline ESM).

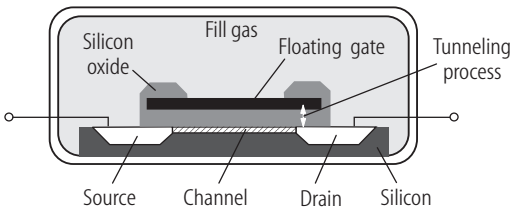

Fig. 10.7. Schematic representation of a DIS dosimeter consisting of combination of a gas-filled ionization chamber and an EEPROM.

10.1.2.3 Proportional counters

A serious limitation of ionization chambers is that they are not sensitive enough to detect individual ionizing particles and thus can not be used for particle counting. This limitation can be overcome by operating an ionization detector in the proportional region to take advantage of the gas amplification process described in Section 10.1.2.1. However, proportional counters are not simply ionization chambers operated at high voltages (predominantly) in the pulse mode, but are specially constructed devices designed to optimize the gas amplification effect [00Kno]. The most important difference is that proportional counters always contain a thin anode wire to create a high electric field. Important geometrical factors are – among others – the uniformity, smoothness, and centricity of the thin anode wire with a diameter of between 5 μm and 50 μm. Specific demands on the gases are: low working voltage, high gas amplification, good proportionality, and high rate capability. These conditions are met by using mixtures of a noble gas and a polyatomic organic gas, such as 90 % argon and 10 % methane (P10 gas) or 96 % helium and 4 % isobutane. The organic additives, denoted as 'quenchers', improve the stability and performance of the counter by absorbing secondary ultraviolet photons – that are emitted from excited gas atoms – in a mode that does not lead to further ionization and thus avoids a transitory electrical breakdown. In practice, gain factors between 10^2 and 10^6 can be achieved.

For particle detection and counting, proportional counters are operated in the pulse mode. Fig. 10.8 shows the equivalent circuit of a proportional counter, which replaces the circuit plotted in Fig. 10.1 for a current-type chamber. As mentioned above, the electrical field increases steeply near the central wire of a ionization detector and thus the amplification process initiated by an ionizing event in the sensitive volume results in an electron 'avalanche' in a region extending only a fraction of a millimeter from the anode surface. However, at the moment when the electrons are collected at the anode wire (within about 1 μs), the positive ions are still so close to the center wire that there is almost no change of the electric voltage. The output signal – a voltage pulse $V(t)$ – is thus predominantly determined by the slower drift of the positive ions outward towards the cathode. Most of this process develops while the ions are still relative close to the wire and thus a sharply defined fast-rising electrical pulse can be observed. The subsequent decrease of the voltage pulse depends on the relative time constant of the external load circuit, which is given by the product of the resistance R and the equivalent capacitance C of both the detector and the measuring circuit (usually a preamplifier). When the capacitance of the circuit is fixed, the height of the voltage pulse is directly proportional to the charge generated within the detector and thus to the amount of energy the incident particle deposited in the gas [00Kno].

Based on this feature, a discrimination between particles depositing different amounts of energy in the gas volume – such as α- and β-particles – can be achieved. This can be realized, for example, by means of two separate read-out channels with different discriminator levels (cf. Fig. 10.8) in order to simultaneously detect either α-particles (high level) or both α- and β-particles (low level). Alternatively, the proportional counter can be connected to a multichannel analyzer, which records and stores pulses according to their height and thus allows the direct discrimination between different particles. If the channel number is related to the energy loss of the incident particles in the cavity by means of a suitable calibration procedure, a proportional counter can also be used for particle identification (particle spectroscopy).

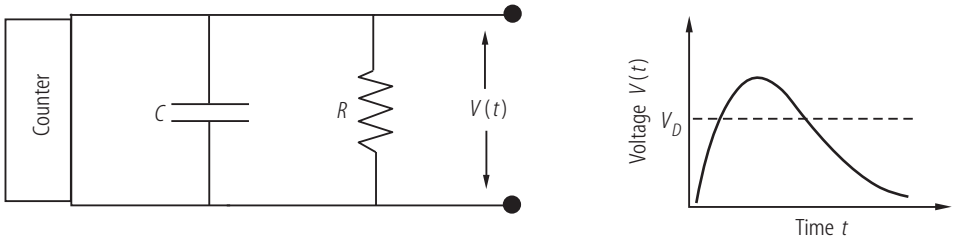

Fig. 10.8. Equivalent circuit of a counter operated in the pulse mode (cf. Fig. 10.1). V_D is the discriminator level. Only pulses with a pulse height exceeding this level are counted.

In practice, it is not possible to record all types and energies of radiation with sufficient efficiency by one detector only and thus different detector designs are used for α-, β-, and γ-radiation. For the detection of α- and low-energy β-particles, it is of particular importance to use counters with thin window foils (such as metalized plastic) or windowless entrance cathodes made of a metal wire grid to reduce absorption or energy-loss of the particles transversing the entrance material as far as achievable. Since such systems can be sealed only heavily, stationary counters are normally operated as gas flow units to avoid gradual contaminations and loss of fill gas. To monitor for contaminations on floors and surfaces of objects in laboratories or on hands, shoes, and clothing of personnel working with radioactive material, large-area proportional counters are used such as those shown in Fig. 10.9. They consist of a cathode container filled with gas, which encloses either a meander-shaped anode wire or multiple anode wires.

Proportional counters (PC) made of a tissue equivalent (TE) plastic wall (most often A-150 plastic) and filled with TE gas mixtures (propane or methane gases mixed with carbon dioxide and nitrogen) are standard instruments in microdosimetry [83ICR]. An important feature of TEPCs, which are based on the Bragg-Gray cavity theory described in Section 10.1.2.2, is that the pressure of the filling gas can be adjusted so that a charged particle crossing the cavity deposits an identical amount of energy as a charged particle crossing a real tissue volume of microscopic dimensions [95Wak]. Multichannel pulse-height measurements with a *low-pressure TEPC* in radiation fields with an intensity low enough to allow the detection of single events thus give the distribution of the energy deposited by individual primary charged particles in a microscopically small tissue volume. Since the height of the recorded pulses strongly depends on the ionization density along the tracks of the charged particles – which varies considerably between different types of charged particles such as electrons, protons and heavier ions – a low pressure TEPC not only acts as recorder of deposited energy, but also as a spectrometer able to distinguish charged particles with a different linear energy transfer (LET) and thus provides an estimate on radiation quality [95Wak, 02Wak].

a

b

Fig. 10.9. Large-area proportional counters for contamination detection. **a:** Sealed handheld monitor for detection of surface contaminations with α-, β- and γ-isotopes. (Courtesy Thermo Eberline ESM). **b:** Continuous gas-flow contamination monitor for detection of α- and β-contaminations of hands, shoes, and clothing. (Courtesy Berthold Technologies).

Low pressure TEPCs have been an important laboratory tool in experimental microdosimetry for many years. The recent availability of microelectronics and progress in digital electronics enabled the development of portable TEPCs for area monitoring and thus the application of this microdosimetric method in practical radiation protection [89Men, 95Sch, 00Sha]. Particular advantages of these devices are the possibility (1) to separate dose fractions due to photons and neutrons in mixed n-γ fields, which release weakly respectively densely ionizing secondaries in the TE wall of the counter, and (2) to directly measure the operational quantity ambient dose equivalent [89Die].

10.1.2.4 Geiger-Müller counters

Although the design and operation of Geiger-Müller (GM) counters are in many respects similar to those of proportional counters, there are three important differences: Firstly, GM counters are operated at substantially higher tube voltages (cf. Fig. 10.2) so that a particle entering the gas volume triggers an electron avalanche extending along the entire length of the anode wire. As a consequence, the size of the output voltage pulses is more or less independent on the number of original ion pairs that initiate the gas amplification process and thus on the type and energy of particle entering the sensitive gas volume. The voltage between the electrodes that is required to sustain an avalanche ionization can be determined by exposing the counter to a constant source of radiation and observing the counting rate as a function of the applied voltage. Secondly, the UV absorbing quench gas used in proportional counters is omitted in GM tubes since ultraviolet photons emitted from excited gas atoms are essential to the process of propagating the discharge throughout the tube. Instead, other 'quenchers' such as gaseous halogens (Cl or Br) or organic substances (ethyl alcohol or ethyl formate) are added with a typical concentration of 5-10 % to the primary fill gas to prevent repeated or continuous gas discharge through the mechanism of charge transfer collisions. A detailed description of the underlying complex mechanism can be found in [86Att, 00Kno]. Thirdly, immediately after a discharge, a dense cloud of positive ions exists near the central wire and reduces the electric field in the counter to a great extent. This space charge not only terminates the discharge of the tube but also prevents that a further avalanche can be generated before the positive ions have moved – at least part of the distance – towards the cathode. The time between the detection of the initial pulse and the time at which a succeeding pulse can be counted because its amplitude exceeds the discriminator level is denoted as resolving time. Typical values are between 100 to 300 μs. In contrast, the resolving time of a proportional counter is less than a few microseconds. During the resolving time, the GM counter is 'dead' and any particles entering the tube during that time are lost [94ICR1].

In practice, gain factors between 10^6 and 10^{10} can be realized with a GM counter. The resulting voltage pulses have a height between 1 and 10 V and can easily be detected with simple electronic circuits – often completely without external amplification. GM tubes are thus simple, rugged, and relatively inexpensive particle-counting instruments. As mentioned above, however, they suffer from extremely long resolving times and are thus seldom used when accurate measurements are required at count rates greater than a few hundred counts per second. In many cases, GM counters are provided with removable covers on the entrance window in order to differentiate between penetrating (γ- and high-energy β-particles) and low-penetrating (α- and low-energy β-particles) radiation by measuring the difference between the count rates with and without the cover in place. As in the case of proportional counters, the entrance window must be sufficiently thin to permit passage of α-particles. For the detection of γ-particles, on the other hand, the thickness of the entrance window or of the cover should approximate the maximum range of the secondary electrons produced in the window or cover to increase detection sensitivity.

10.1.3 Scintillation detectors

The major limitation of gas-filled counters, namely the low detection efficiency for X- or γ-rays, can be overcome by the use of solid or liquid detector materials, which have a much higher density than gases. Scintillation materials are frequently utilized for photon or neutron detection. In these materials a small fraction of the energy deposited by charged particles will be emitted as visible or ultraviolet light on a time scale of nanoseconds to milliseconds, whereby the intensity of the light flash is proportional to the energy deposited in the scintillator. As shown in Fig. 10.10, a scintillation detector consists basically of scintillator material that is optically coupled to a photomultiplier tube to convert the light photons released in the scintillator into an electrical pulse which can then be amplified and analyzed electronically.

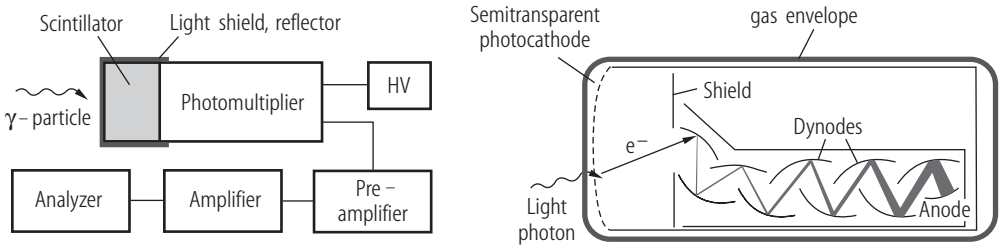

Fig. 10.10. Schematic representation of **(a)** a pulse-mode scintillation detector and **(b)** a linear focussed photomultiplier tube showing the cascade effect due to amplification of electrons from the photocathode by increasing secondary emission when the electrons strike the dynodes.

Scintillators fall into two major categories: inorganic and organic materials, the choice of which depends strongly on the type of measurement to be performed. Physical properties of a few representative scintillator materials are given in Table 10.3; a more comprehensive list can be found in [00Kno, 94Leo].

Inorganic scintillators are crystals of alkali halides (such as NaI, CsI) or oxides (such as $Bi_4Ge_3O_{12}$, 'BGO') grown at high temperatures. In these materials, scintillation is a property of the electronic band structure of the crystals: When an ionizing particle enters the scintillator, it can raise electrons from the valence into the conduction band. The electrons and holes formed by this excitation process recombine and emit a photon. In the pure scintillator material, however, de-excitation is an inefficient process due to self-absorption. Therefore, small amounts of an 'activator' (e.g., thallium in the case of NaI) are added. These impurities create energy states within the forbidden band gap of the scintillator over which electrons can alternatively de-excite from the conduction band into the valence band. A more detailed description of the scintillation process can be found in [00Kno, 95Tso]. Since energy spacing between activator energy states is less than that between the conduction and valence bands of the pure solid, the emitted photons do not have enough energy to raise other electrons from the valence band to the conduction band and thus cannot be effectively reabsorbed by the scintillator. Moreover, the change in energy of the emitted photons results in a shift of the wavelength of maximum emission from the ultraviolet into the visible region, where the sensitivity of most photomultiplier tubes is maximal. Inorganic scintillators tend to contain elements with a high atomic number and have a relatively high density (cf. Table 10.3). Consequently, the photoelectric effect is the main interaction mechanism for X- or γ-rays in the energy range between 10 keV to 1 MeV, making inorganic scintillators favorable for particle identification by means of spectroscopic measurements (see below). They also have a high light output, but are hampered by a relatively slow response.

Organic scintillators, on the other hand, are aromatic hydrocarbon compounds which contain benzenoid rings. They are broadly classed into three types: crystalline, liquid, and plastic, all of which utilize the ionization produced by charged particles to generate optical photons, usually in the blue to green wavelength regions. Examples of pure organic crystals are anthracene ($C_{14}H_{10}$) and trans-stilbene ($C_{14}H_{12}$). Plastic scintillators are non-fluid solutions consisting of fluorescent organic compounds dis-

solved in a solidified polymer matrix or fluid solutions with similar fluorescent organic compounds [02Sai]. In contrast to inorganic scintillators, the fluorescence process in organic scintillators is an inherent molecular property which is characterized by the excited states of the individual molecules. Therefore, fluorescence can be observed independent of the physical state of the material. Organic scintillators are generally faster in their response than inorganics and are more suitable for β-particle spectroscopy and especially for fast neutron detection due to the high hydrogen fraction in their composition (cf. Section 10.1.7). Moreover, some organic scintillator materials (such as BC 501 / NE 213, cf. Tab. 10.3) offer the possibility to discriminate between photons and neutrons due to differences in scintillator response. In these materials, electrons released by γ-quanta cause scintillations at a rate faster than that due to photons created by neutrons.

Table 10.3. Physical properties of a few representative scintillator materials (data from [02Sai]).

Material	Type	Density	Refraction index	Light output[a]	Decay constant[b]	Wavelength[c]	Main application
		[g/cm^3]		[%]	[ns]	[nm]	
Inorganic scintillators							
NaI(Tl)	Crystal	3.67	1.85	100	250	415	γ, X-rays
CsI(Tl)	Crystal	4.51	1.79	45	1005	550	γ, heavy particles
CsI(Na)	Crystal	4.51	1.84	85	630	420	γ, heavy particles
BGO	Crystal	7.13	2.15	20	300	480	γ, X-rays
LSO	Crystal	7.40	1.82	63	40	420	γ, X-rays
Organic scintillators							
Anthracene	Crystal	1.25	1.62	100	30	447	General purpose
Trans-stilbene	Crystal	1.16	1.63	50	4.5	410	γ, fast n
BC 400 / NE 102	Plastic	1.03	1.58	65	2.4	423	General purpose
BC 422 / NE 111	Plastic	1.03	1.58	55	1.6	370	Ultra-fast timing
BC 501 / NE 213	Liquid	0.87	1.51	78	3.2	425	Fast n with γ discrimination
BC 509 / NE 226	Liquid	1.61	1.38	20	3.1	435	γ, insensitive to n

[a] Given relative to NaI(Tl) for inorganic scintillators and relative to anthracene for organic scintillators. The light output of anthracene is 40-50 % of NaI(Tl). [b] Main component. [c] Maximum emission.

As mentioned above, photomultiplier tubes (PMT) have two different functions: conversion of ultraviolet and visible photons emitted by the scintillator into an electrical signal and signal amplification. Fig. 10.10 shows the essential parts of a PMT, which are mounted inside an evacuated glass envelope, namely a photocathode, typically 10 to 12 electrodes denoted as dynodes, and an anode. The photons from the scintillator strike the photocathode – usually made of a semiconductor material formed from antimony plus one or more alkali metals – and release photoelectrons with an efficiency of about 10-30 % [94Leo]. These photoelectrons are attracted to the first dynode, which is at a higher potential than the cathode, so that the electrons strike the dynode with a sufficiently high kinetic energy to eject three to four secondary electrons from the surface. Since each dynode has a more positive voltage than the preceding one, this amplification process is repeated with each successive dynode, so that a multiplication factor of 10^6 or more can be obtained with a twelve stage PMT. The average gain of the dynode chain is independent of how many electrons are simultaneously ejected from the photocathode. As a consequence, the size of the electrical output signal at the anode is proportional to the number of electrons leaving the photocathode. To achieve a good performance, it is important to match the emission spectrum of the scintillator to the quantum efficiency of the photocathode material. The current measured at the anode of the PMT is fed into an RC circuit as shown in Fig. 10.8 to produce an electrical voltage pulse.

The previous discussion reveals, that the output of a scintillator-PMT combination is proportional to the amount of energy deposited by an incident particle in the scintillator and can thus be used for *particle spectroscopy*. To this end, the voltage pulse goes into an amplifier and is then fed into a multichannel analyzer, which records and stores pulses according to their voltage amplitude into different channels. By using γ-ray sources of known energy, the channel numbers can be related to energy. As an example, Fig. 10.11 shows the pulse-height spectrum of ^{60}Co recorded from a large NaI(Tl) scintillator.

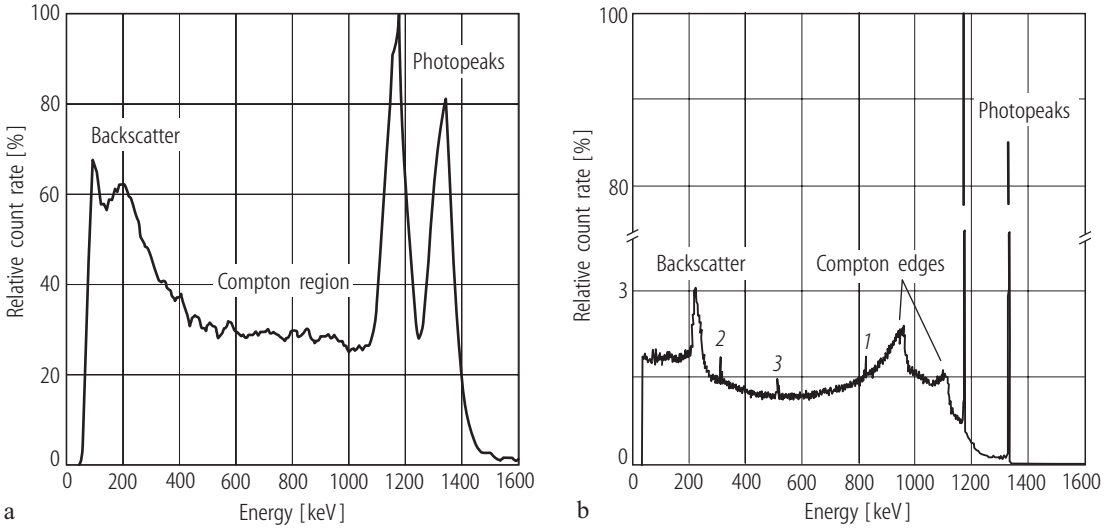

Fig. 10.11. Pulse-height spectra of ^{60}Co measured with **(a)** a large NaI(Tl) scintillation detector and **(b)** a high-purity germanium detector. The two characteristic photopeaks are at energies of 1.17 and 1.33 MeV. In (b) a single (1) and a double escape peak (2) related to the incident 1.33-MeV-photons is apparent, as is an annihilation peak at 511 keV (3) due to pair production interactions in surrounding materials. Note that incident 1.17-MeV-photons do not give rise to escape peaks, since the photon energy is only slightly above the threshold for pair production interactions where the cross section is still very low.

A pulse-height spectrum recorded from a radiation source depends not only on the characteristics of the radiation to be measured but also on the type of scintillator used and the mechanisms by which the incident particles transfer their energy to the detector material. Since the ranges of charged particles are very short in most solid and liquid materials, they deposit their energy almost completely in the detector material giving rise to a well-defined peak in the spectrum at the particle energy. In the case of γ-quanta, energy is deposited to the detector primarily by the photoelectric effect, Compton scattering, and pair production. An incident photon undergoing a photoelectric interaction in the scintillator transfers (nearly) all of its energy to an electron and thus contributes to the 'photopeak' in the pulse-height spectrum, which is located at the energy of the incident photon. In Compton scattering, however, only part of the energy is transferred to the detector, via the recoil electrons. The scattered photon may either be absorbed by a photoelectric interaction within the scintillator or may escape from the detector. In the first case, the total energy of the incident photon is absorbed and the event will contribute to the photopeak. In the second case, however, the energy deposited by the recoil electron depends on the scattering angle. The 'Compton region' in the spectrum thus ranges from near zero (small-angel scattering) up to a maximum energy ('Compton edge') for 180° Compton scattering. If the energy of the incident photon exceeds 1022 keV, pair production can occur. When the positron created by this process comes to rest, it combines with an electron to create a pair of 511 keV annihilation photons. If one or both of these photons escape, the energy deposited in the scintillator is reduced by 511 or 1022 keV, respectively. As a consequence, additional 'photopeaks' – denoted as single and double escape peaks – appear in the spectrum at energies of 511 keV and of 1022 keV below the corresponding full-energy photopeaks (cf. Fig. 10.11). Finally, low-energy peaks may appear in the spectrum resulting from γ-quanta that are scattered in material outside of the scintillator, and enter the detector having lost most of their energy. However, these backscatter peaks

area usually easy to identify due to their low energies (<250 keV). Since both the energy and relative emission probability of γ-rays released by a radioactive decay is a characteristic property of nuclides, γ-spectroscopy is widely used for the identification of nuclides in a sample or in the environment [94ICR2]. A discussion of the various aspects related to particle spectroscopy can be found in [00Kno, 95Tso].

Scintillation detectors not only have a markedly higher detection efficiency for γ- or X-rays than gas-filled ionization detectors due to the higher density of the detector material but also a much shorter resolving time which allows them to respond more linearly to higher count rates than Geiger-Müller counters. Therefore, scintillation counters are frequently applied for particle counting and identification. As an example, Fig. 10.12 shows a portable NaI spectrometer for the localization, identification, and measurement of γ-rays. A major limitation of scintillation detectors, on the other hand, is their poor energy resolution. The reason is that an average energy loss of 100 eV or more in the scintillator material is required to release one photoelectron from the photocathode of the PMT and that, consequently, the average number N of photoelectrons – or information carriers – produced by an incident ionizing particle is no more than a few thousands. Due to the random nature of the interaction processes, the standard deviation characterizing the statistical fluctuations in that number is proportional to $\sqrt{N}$ and the relative uncertainty proportional to $1/\sqrt{N}$. Therefore, there is a significant inherent limitation on the energy resolution of scintillation counters [00Kno]. For example, scintillation detectors used in γ-spectroscopy typically show an energy resolution in the range of 5 - 10 % (cf. Fig. 10.11a). The intrinsic statistical limit on energy resolution can only be reduced by increasing the number of information carriers created per unit energy lost by the incident radiation – as, for example, by the use of semiconductor materials.

Fig. 10.12. Portable NaI spectrometer with 496 channels for the localization, identification, and measurement of γ-rays with an energy between 25 keV and 2 MeV. (Courtesy Berthold Technologies).

10.1.4 Semiconductor detectors

Semiconductor detectors have experienced a rapid development in the last decades. They are basically solid-state analogs of gas-filled ionization detectors, in which electron-hole pairs are created by incident ionizing radiation instead of electron-ion pairs.

Semiconductors are made of crystalline materials whose electrical conductivities are midway between those of conductors and insulators. Their electrical properties are characterized by their crystal structure: According to quantum theory, the energy of an electron in the crystal must fall within well-defined bands – the valence or the conduction band, which are separated by a forbidden energy gap. The most common semiconductor materials used are silicon and germanium which crystallize in the diamond structure (Table 10.4). In this structure, the four valence electrons form covalent bonds with each of the four nearest neighbor atoms in the crystal and are thus – at least at very low temperatures – immobile. The

energy gap between the valence and conduction band is, however, much smaller in semiconductors (about 1 eV) than in insulators (more than 5 eV) and thus ionizing radiation, light, or heat can easily break covalent bonds and raise electrons into the conduction band, leaving behind electron vacancies or 'holes' in the valence band. When an electric field is applied across a semiconductor crystal, 'free' electrons in the conduction band and positive 'holes' in the valence band, which act as positive charge carriers, move towards the positive and negative terminal, respectively, and establish a small current when the terminals are connected to a detection circuit. The problem is, however, that at non-zero temperatures electron-hole pairs will be thermally generated in the semiconductor material and that the random fluctuations that unavoidably occur in the resulting steady-state leakage current are too high, even in the highest resistivity materials available, to permit the detection of the minute current caused by electron-hole pairs initiated by an ionizing particle. This problem can be solved by using the favorable properties of a *p*-*n* semiconductor junction, which acts as 'blocking' contact with an extremely high resistance and thus reduces the leakage current through the bulk of the semiconductor material.

Table 10.4. Physical properties of silicon and germanium (data from [95Tso] and [99Lut]).

Property		Silicon	Germanium
Atomic number		14	32
Atomic weight		28.1	72.6
Density at 300 K	[g/cm^3]	2.33	5.32
Energy gap at 300 K	[eV]	1.11	0.67
Intrinsic resistivity at 77 K	[Ω m]	∞	500
Intrinsic resistivity at 300 K	[Ω m]	2300	0.47
Average energy per electron-hole pair at 77 K	[eV]	3.7	2.96
Average energy per electron-hole pair at 300 K	[eV]	3.65	–

To this end, a pure semiconductor is doped on one side with pentavalent impurity atoms (for example, phosphorus, antimony, or lithium) and on the other side with trivalent impurity atoms (for example, boron, gallium, or indium). When present in small concentrations, the impurity atoms will take the place of a tetravalent normal silicon or germanium atom in the lattice and introduce only lightly bounded excess electrons or additional electron vacancies (holes) in the crystal lattice, respectively. A semiconductor material containing an electron-donor impurity is denoted as *n*-type material, material doped with a hole-forming impurity as *p*-type material. As already mentioned, the essential part of a semiconductor detector or diode is the region in the vicinity of the interface between the *p*-type and *n*-type material, which is denoted as *p*-*n* junction. Due to the difference in the concentration of electrons and holes between the two materials, electrons diffuse into the *p*-region and holes into the *n*-region. As a consequence, the diffusing electrons fill up holes in the *p*-region while the diffusing holes capture electrons on the *n*-side, leaving a region completely depleted of mobile charge carriers, as schematically shown in Fig. 10.13. Since *p*- and *n*-type materials are originally electrically neutral, the diffusion process creates a net negative and positive space charge on the *p*-side and *n*-side of the junction, respectively. At equilibrium, the electric diffusion potential (about 0.5 - 1 V) across the *p*-*n*-junction results in the transport of charge carriers in the opposite direction which precisely balances the diffusion process of charge carriers and limits the extension of the depletion region to rather small depths (about 50 to 100 μm). However, the region where the electric field exist – and thus the depletion depth – can be increased by applying a strong reverse-bias voltage across the semiconductor, as illustrated in Fig. 10.13. It is important to note, that thermal generation of electron-hole pairs in the depletion region does not result in a considerable steady-state concentration of carriers because removal of these carriers is a much faster process than their creation. Therefore, the small concentration of carriers created by ionizing particles can easily be detected above the highly suppressed concentration of thermally generated carriers [00Kno].

Pure semiconductor crystals, referred to as wafers, are grown from the melt of high-purity polycrystalline silicon or germanium material with the help of a seed crystal of defined orientation. A *p*-*n* junction detector is usually produced by depositing sufficient *p*-type impurities into one end of a uniformly *n*-doped wafer so as to change that end into a *p*-type material. This can be done either by diffusion or implantation of dopants, or by a combination of both processes. A more detailed description of the fabrication and design of semiconductor detectors and of their application is presented in [99Lut].

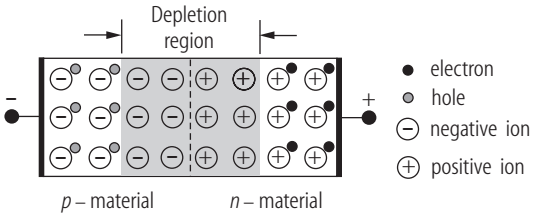

Fig. 10.13. Schematic representation of a *p*-*n* detector or diode. At the junction, electrons diffuse into the *p*-region and fill up holes while holes diffuse into the *n*-region and capture electrons. This process results in a region completely depleted of mobile charge carriers (grey area). By applying a reverse-bias voltage, the depth of the depletion region is increased.

For particle spectroscopy, semiconductor detectors are operated in the pulse counting mode. As in the case of a scintillation detector, the charge created in the detector material is transformed by means of a charge sensitive preamplifier stage into a voltage pulse, the height of which is proportional to the energy deposited by an incident ionizing particle in the depletion region. The energy resolution of a semiconductor detector, however, is much better than that of a scintillation counter, since the average energy required to produce an electron-hole pair in a semiconductor material (about 3 eV, cf. Table 10.4) is much smaller than the average energy required to release a photoelectron from the photocathode of the PMT (more than 100 eV). The superior energy resolution is demonstrated by the comparative pulse-height spectra of ^{60}Co plotted in Fig. 10.11. Whereas silicon is the most widely used semiconductor material for charged particle detection, germanium is the preferred material for γ-spectroscopy because of its much higher atomic number (cf. Table 10.4) and thus its greater photoelectric cross section. In contrast to silicon, however, germanium must be operated at cryostatic temperatures because of its relatively narrow energy gap between the valence and conduction band. A principal drawback associated with all semiconductor detectors is the degradation in performance which can be brought about by radiation damage.

At low energies, the efficiency of semiconductors for γ-detection is a function of photon cross-section and window thickness, whereas at higher energies the total active detector volume becomes the most important factor. Germanium detectors can be fabricated in many different geometries thus offering devices that can be tailored to the specific needs of the measurement [cf. 95Tso]. With the exception of the well-type configuration, the efficiency of germanium detectors is low relative to Na(Tl) scintillators. This is, however, more than compensated for by the better energy resolution. As representative examples, Fig. 10.14 shows detector efficiency and energy resolution curves for various types of germanium detectors. To take full advantage of their intrinsic energy response, detectors with thin contacts – such as low-energy germanium (LEGe) and reverse electrode germanium (REGe) detectors – are usually equipped with a beryllium cryostat window.

In the last decade, compound semiconductors have gained increasing interest as detector materials applicable to γ-spectroscopy [00Kno]. Particularly cadmium zinc telluride (CdZnTe) based detectors have been developed intensively and have recently seen significant improvements [01Tak]. These devices offer some major advantages: operation at room-temperature due to the wide band gap of the material, a resolution that is intermediate between that of scintillation detectors and germanium devices, and a high density of the crystal providing excellent stopping power over an energy range of a few keV to over 1 MeV. Based on these features, portable γ-spectrometers have been developed for radiation protection measurements.

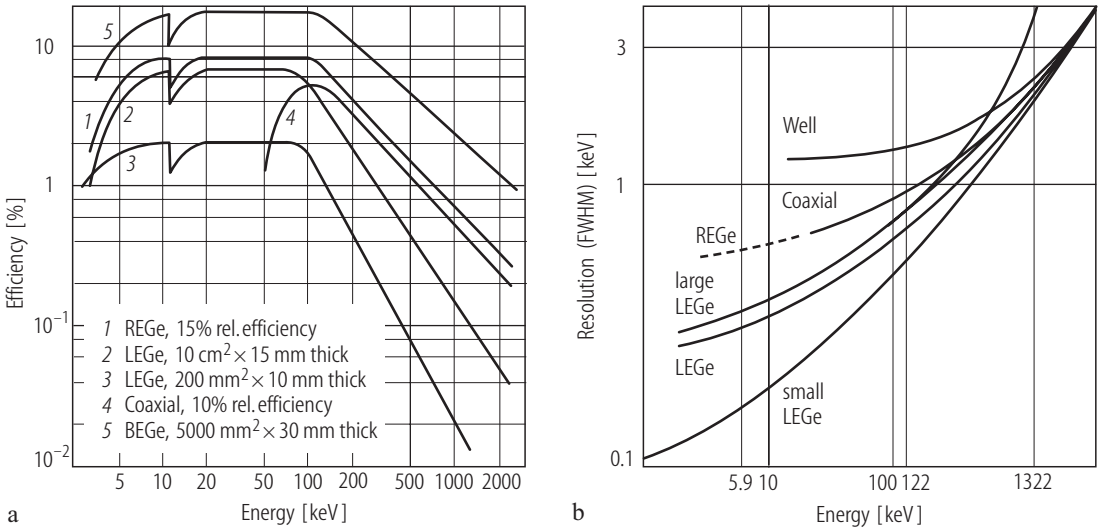

Fig. 10.14. Typical performance parameters for various types of germanium detectors frequently used for γ-spectroscopy. **(a)** Absolute detector efficiency as a function of energy compared to that of a 37×37 mm^2 Na(Tl) crystal at a detector to source distance of 25 cm. **(b)** Energy resolution (full-width at half-maximum, FWHM) as a function of photon energy. Well: well-type Ge detector, REGe: reverse electrode Ge detector, LEGe: low-energy Ge detector, BEGe: broad energy Ge detector, Coaxial: coaxial Ge detector. (Figures adapted with permission from Canberra Industries).

Fig. 10.15. Direct-reading electronic personal dose and dose rate meter for measurements of X- and γ-rays over the energy range from 60 keV to 3 MeV with an accuracy of the dose reading of ± 15 % between 1 μSv and 10 Sv. The detector system, which utilizes an energy compensated silicon diode, is calibrated to give directly the personal dose equivalent $H_p(10)$. (Courtesy Rados Technology).

With recent improvements in their applicability and reliability, silicon (PIN) diodes have also become popular as radiation detectors in *electronic pocket dosimeters* (cf. Fig. 10.15). To measure the absorbed dose, it is more appropriate to operate these devices in the current mode, since the current measured with a silicon diode is nearly proportional to the absorbed dose rate in soft tissue for photon energies between 150 keV to well over 1 MeV. The reason is that the mass absorption coefficients for silicon is within 10 % of soft tissue values over the given range of photon energies and thus conversion of photons into energetic electrons is similar in both cases [00Kno]. At lower energies, however, photon absorption in silicon deviates considerably from that in tissue. It is thus necessary to compensate for this effect by employing metallic filters around the detector. There are different approaches to realize energy compensation: One approach, which is designed to measure both γ-quanta and β-particles, is to use three diodes in parallel with individual filters to produce an appropriate energy response that is approximately energy-independent down to about 17 keV [95Hir]. A more cost effective solution is to use a single diode with a simple filter, usually tin, to flatten the energy response – with the major disadvantage of giving up response to photons with an energy below about 60 keV. By using a composite filter of two or more filters together with several openings, however, it is not only possible to compensate the energy response of a silicon diode but also to maintain an extended low energy response [96Ols]. As compared to passive personal monitoring devices such as photographic films or thermoluminescence dosimeters, described in the subsequent sections, electronic personal dosimeters offer various advantages, such as real-time

measurement and display of the dose rate and cumulative dose, audible warning of radiation fields at user settable alarm levels, and the possibility to transmit data for remote readout and evaluation by dosimetry management system.

10.1.5 Thermoluminescence and radiophotoluminescence detectors

The use of *thermoluminescence detectors* (TLDs) is another common method of solid-state dosimetry based on the electrical properties of crystals. In these crystals, too, electrons are raised by ionizing radiation from the valence into the conduction band. In contrast to scintillation materials, however, the electrons and holes formed by the excitation process do not recombine immediately but are caught in 'traps' for long periods of time at room temperature, as shown in Fig. 10.16. Whereas in some natural materials traps are formed by lattice imperfections and impurities inherent to the crystal, small concentrations of impurity (e.g., Mn, Ti, Tm, Mg, Dy) must be added in others, which function as an activator. Some TL materials commercially available are $CaSO_4$:Mn, CaF_2, CaF_2:Mn, CaF_2:Dy; $Li_2B_4O_7$:Mn, LiF, LiF:Mg, Ti, and LiF:Mg, Cu, P (activators are given after the colon). The choice among TL materials depends on different factors: (1) the energy depth of the traps, which determines the number of charge carriers trapped per unit of absorbed dose and thus the sensitivity of the TL detector, (2) the retention of the trapped carriers for longer periods of time at normal temperatures, and (3) linear response over a large dose range.

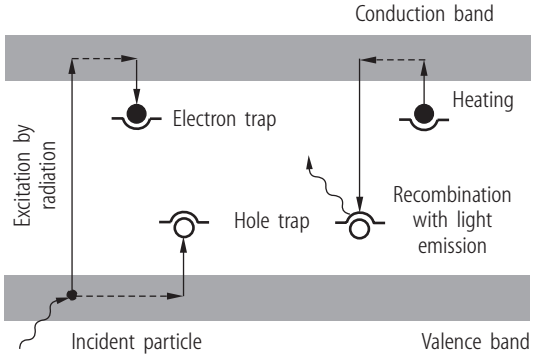

Fig. 10.16. Energy-level diagram of a TLD crystal. **Left:** Radiation induced formation of an electron-hole pair leading to the population of an electron and a hole trap. **Right:** Release of a trapped electron by heat and subsequent recombination with a hole resulting in the emission of a photon. It is assumed that the electron is liberated first since the depth of the electron trap is less than that of the hole trap. In the reverse case, the hole would be thermally released first. The dashed lines represent drift of charge carriers in the valance and conduction band.

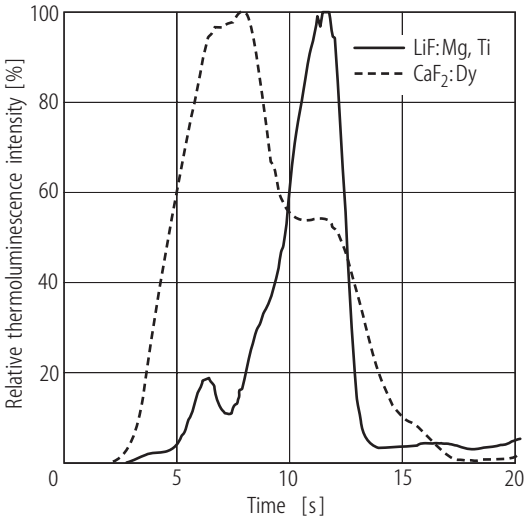

Fig. 10.17. Representative thermoluminescence glow curves of LiF:Mg, Ti (TLD-100) and CaF_2:Dy heated from 50 °C to 325 °C within 20 s. The curves are normalized to the same maximum intensity.

The charge carriers stored in a TLD after having been exposed to radiation can be released by heating the detector, e.g., by a stream of heated gas, by laser light, or by heating the support. As schematically shown in Fig. 10.16, this process provides sufficient thermal energy to electrons or holes so that they are raised back into the valence or conduction band, respectively. 'Free' electrons (or holes) can migrate towards the position of a trapped hole (or electron) and recombine with the emission of light. The photons emitted by the heating process are detected by a photomultiplier tube (PMT) as in the case of a scintillation detector (cf. Section 10.1.3). The PMT output signal, which is proportional to the number of photons released in the TL material, is detected and plotted as a function of temperature or time during heating

with a constant rate. The resulting plot is denoted as 'glow' curve, which may consist of various resolved or unresolved glow peaks if there are several types of traps in the TLD material – each of which is characterized by a specific depth or binding energy (Fig. 10.17). The area under either the entire curve or individual peaks is a measure of the number of trapped charge carriers and thus of the amount of energy absorbed in the crystal. Determination and analysis of glow curves are performed by dedicated devices denoted as TLD readers (Fig. 10.18). Since the intrinsic TL efficiency, i.e. the ratio between the light energy emitted per unit of detector mass and the absorbed dose, is in the order of 1 % only, TLDs must be used under reproducible conditions to obtain consistent results. One important aspect is to thoroughly deplete all traps in the detector before it is reused for dose measurements. To this end, the temperature of TLDs must be raised to relatively high values over longer periods of time in an annealing oven (cf. Fig. 10.18). TLD dosimetry is a relative measurement technique and thus TLDs have to be calibrated individually against absolute dosimetry systems such as a calibrated ion chamber. Details on TLD dosimetry and calibration are presented in [86Att, 00Sha].

TLDs are available in diverse forms – such as loose powder, chips, rods, rings, or small wafers – and are widely used as single element dosimeters or assemblies for a large variety of radiation protection measurements (Fig. 10.18). They have found, for example, an important place in personal monitoring and are rapidly replacing the use of photographic films discussed in the next section. In personal monitoring devices, one or more small TLD elements are usually assembled into rigid aluminum cards and mounted within shielded filter-holders. For this and many other purposes, LiF:Mg, Ti is the material of choice because it is approximately tissue-equivalent (effective atomic number of 8.2 compared to 7.4 for tissue) and almost energy-independent for photons with an energy between 0.1 and 3 MeV [86Att]. Moreover, it is to some extent sensitive to thermal neutrons, since natural lithium (TLD-100) contains to 7.4 % ^{6}Li that has a high (n,α) capture cross section. The response to neutrons can be enhanced or reduced by using ^{6}Li (TLD-600, with 96.5 % ^{6}Li) or ^{7}Li enriched material (TLD-700, with 99.99 % ^{7}Li) (cf. Section 10.1.7).

Fig. 10.18. **(a)** TL detectors for radiation protection measurements (chips, rods, and ring). **(b)** TLD reader for the evaluation of irradiated detectors. **(c)** Annealing oven for the preparation of the detectors. TL detectors are placed in a metallic container which comes into contact with two heating plates to ensure optimal thermal equilibrium. (Courtesy PTW Freiburg).

In some substances – such as BeO, LiF, Al_2O_3, $CaSO_4$, and some alkali halides – electrons liberated during the heating procedure may also have a chance to leave the material when the trap sites are located in a thin (<10 nm) surface layer. This process, that is closely related with the conventional TL mechanism [99Sak], is referred to as *thermally stimulated exoelectron emission* (TSEE). The low energy exoelectrons can be detected, for example, by a windowless proportional or Geiger-Müller counter (cf. Section 10.1.2.3 and 10.1.2.4, respectively). The number of exoelectrons detected is proportional to the dose in the surface layer. TSEE dosimetry has gained interest since it can be used for the measurement of weakly penetrating radiation, such as low energy γ-quanta or α- and β-particles [86Sch].

A limitation of conventional TLD technology is the complete annealing of populated traps, when the material is heated during the readout process. Therefore, alternative luminescence techniques have been investigated that permit successive readouts and the construction of integrating dosimeters. An approach that has been applied more frequently in health physics is based on the optical phenomenon of *radio-photoluminescenc*e (RPL) [68Att, 87Per]. RPL is a property of certain substances to emit fluorescent light

in the visible range upon irradiation with ultraviolet light, when the substance has previously been exposed to ionizing radiation. Although various materials exhibit this property, silver-activated metaphosphate glasses are most commonly used. In RPL glasses, ionizing radiation results in the formation of stable fluorescing centers that emit orange light (about 640 nm) under (pulsed laser) ultraviolet stimulation (365 nm) [93Pie]. The intensity of fluorescence light, which is determined with a spectrally matched PMT as in the case of traditional TLD readout, is proportional to the number of light centers and hence to the radiation dose. Since the light centers are not destroyed by ultraviolet excitation, the readout procedure can be repeated as often as necessary. For practical application as personal dosimeters, optimized RPL ('Yokato') glasses are covered with metal filters or capsules which provide largely energy-independent dose measurements for γ-quanta with an energy above 50 keV [72Kie, 96Hoh].

10.1.6 Photographic films

Film dosimetry is an attractive technique for many applications – especially in medical physics – due to its high spatial resolution, wide accessibility, and the flexibility to place the film in humanoid phantoms [00Sha]. Furthermore, photographic films are still widely used for monitoring radiation exposure of personnel although they do by no means meet the requirements of an ideal personal dosimeter in all respects. Photographic films consist of an emulsion of microscopic grains of silver halides, usually silver bromide, dispersed in a gelatine layer on one or both sides of a transparent film base of cellulose acetate or polyester. The photographic process is very complicated. A thorough discussion of the complex experimental and theoretical aspects, which are considerably simplified in the following description, can be found in [02Bus] and [81Bar], respectively. When the silver bromide grains in the emulsion are exposed to visible light or ionizing radiation, bromide ions absorb energy and are oxidized. The electrons from this oxidation process reduces silver ions to silver atoms. Experimental evidence indicates that a minimum of three to five reduced silver atoms form a 'sensitized' grain, that can act as a catalyst for the chemical amplification process during film development. When the film is placed in a chemical developer solution, all silver ions in the grains will be reduced to silver atoms – independently of whether the grains were affected by ionizing radiation or not. Silver atoms in 'sensitized' grains, however, greatly enhance the rate of reduction of additional silver ions. Based on this fact, the chemical development process is terminated after a time at which the reduction process in 'sensitized' grains is completed by taking the film out of the developer solution and placing it in a fixing solution that neutralizes residual developer present on the film. The chemical development process greatly increases the number of silver atoms and makes the radiation effect measurable. To ensure reproducibility of the results, careful control of the developing procedures is essential.

The degree of macroscopic blackening of the processed film depends on the number of silver atoms deposited and thus on the amount of energy absorbed. It is usually expressed in terms of the optical density OD which is defined in terms of the transmission of light through the film as $OD = \log_{10}(I_0/I)$, where I_0 and I are the intensities of a light beam measured by an optical densitometer in front and behind the film. The relation between the optical density of the film and the exposure is described by the 'characteristic curve' for the particular film – typically a sigmoid-shaped curve with three characteristic regions: At low exposures, the optical density is low and independent of exposure level. Next, there is a segment over which the optical density and the logarithm of the exposure are approximately linear related. This is the region of normal operation. In the third segment, which corresponds to large exposures, the film becomes saturated since all silver ions are converted to metallic silver [81Bar].

The response of photographic films is strongly dependent on radiation energy. For photon energies below 100 keV, for example, the relative sensitivity is between 10 and 50 times higher than at higher energies [86Att]. In order to flatten the energy response, film badge dosimeters contain a set of metallic filters of various materials and thicknesses over different regions of the film as shown in Fig. 10.19. By comparison of the optical density behind these filters, it is possible to get rough spectral information

which can be utilized to take the energy dependence of the film's sensitivity approximately into account. Disadvantages of film badge dosimeters are, firstly, the considerable angular dependence of the detection efficiency and, secondly, fading of 'sensitized' grains in the period between exposure and development [72Kie]. Both effects can result in a considerable underestimation of radiation exposure.

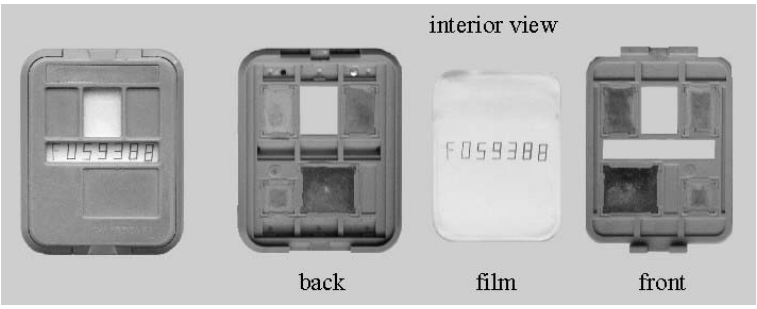

Fig. 10.19. Film-badge dosimeter for personal monitoring. The interior view of the holder shows at the back and front an open window, three copper filters of different thickness, and a staggered lead / tungsten filter to identify the direction of the incident radiation. The light-tight wrapping contains two dosimetry films of different sensitivities.

10.1.7 Detectors for neutrons

In the previous sections, devices for the detection of photons and charged particles have been described, which deposit their energy in matter predominantly via electromagnetic interactions – in particular by inelastic collisions with the atomic electrons. In contrast, the interaction of fast neutrons with matter occurs through processes with the nucleus, e.g. elastic or inelastic scattering or various nuclear reactions. The most important nuclear reactions for the detection of neutrons in the eV to keV region are (n,α) and (n,p) reactions, such as ^{6}Li (n,α) ^{3}H, ^{10}B (n,α) ^{7}Li, or ^{3}He (n,p) ^{3}H, in which a neutron is captured and a charged particle is released. These substances have a high sensitivity at low neutron energies, which is of particular advantage considering the low dose rate levels routinely encountered in radiation protection, but become more and more ineffective at higher neutron energies E because the capture cross sections vary as $1/\sqrt{E}$. Instead, elastic scattering of neutrons at nuclei becomes the most relevant interaction mechanisms, giving rise to recoil nuclei. Whereas the energy transfer to a recoil nucleus is very ineffective in the case of heavy nuclei, an incident neutron can transfer up to its entire energy in a single collision to a hydrogen nuclei (proton) because neutrons and protons have nearly the same mass. Therefore, detectors with a high content of hydogen in the detector or cover material are used for neutron detection by measuring the recoil protons. In addition, hydrogen-containing materials, so-called moderators, can be utilized for slowing down of fast neutrons to thermal energies. A more quantitative discussion of the various interaction processes, by which neutrons transfer all or part of their energy to charged particles capable of exciting and ionizing, can be found in [72Kie, 00Kno, 94Leo].

A sensitive and simple *counting device* for slow neutrons is a proportional counter filled with BF_3 gas, usually enriched to more than 90 % in ^{10}B. In such a counter, BF_3 gas not only serves as the target for slow neutron conversion into α-particles via the above mentioned ^{10}B (n,α) ^{7}Li reaction but also as filling gas. Since α-particles yield a much higher output signal than γ-particles, BF_3 counters can be used to discriminate between the neutron and γ-component in a mixed n-γ field (cf. Section 10.1.2.3). By sourrounding the counter by a moderating material (e.g. paraffin or polyethylene) in which the neutrons are slowed down, it can also be utilized for the detection of fast neutrons. An alternative approach for the detection of slow neutrons is the use of proportional counter, the walls of which are coated with a layer of B_2O_3 or BC_4. Such 'boron-lined counters' offer the flexibility to use more appropriate filling gases than BF_3 [00Kno, 95Tso].

A particular problem in neutron dosimetry is the broad energy range that can occur and the considerable variation of detector response over this range. Nevertheless, dosimeters for routine *area monitoring* can be constructed in such a way that the shape of their fluence response as a function of energy approximate that of the fluence-to-dose equivalent conversion function and thus will give a reading approximately proportional to the ambient dose equivalent $H^*(10)$ over most of the energy range of interest

(cf. Section 4.5.3.3 and [01ICR]). To this end, thermal-neutron detectors are surrounded by a moderator, whose material and geometry is chosen to optimize the desired response function. A widely used survey instrument is the 'rem counter' shown in Fig. 10.20. It consists of a massive sphere with a diameter between 25 and 30 cm of hydrogenous material – usually polyethylene with additional layers of cadmium or boron – that serves as neutron moderator surrounding a thermal-neutron detector, e.g. a ^{3}He proportional tube. An extension of this approach is the 'Bonner sphere' spectrometer, which uses different moderator spheres with diameters ranging from 5 to 30 cm. Since the response functions for the diverse moderator spheres differ in shape and position of the maxima, the energy distribution of a neutron field can be derived from count rate measurements performed separately for each of the spheres [00Kno, 00Sha].

Fig. 10.20. Dose rate monitor ('rem counter') for the measurement of neutron ambient dose equivalent $H^*(10)$ for neutrons up to an energy of 20 MeV. The detector system consists of a proportional counter tube centered in a moderator sphere with a diameter of 250 mm. (Courtesy Berthold Technologies).

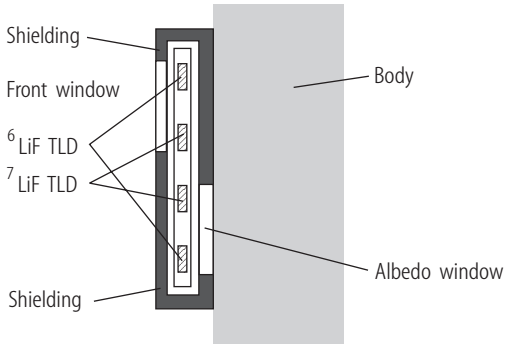

Fig. 10.21. Schematic representation of an albedo TLD dosimeter consisting of two pairs of ^{6}LiF - ^{7}LiF detectors that are shielded by cadmium- or boron-loaded material either against incident thermal neutrons or albedo neutrons from the rear.

As described in Section 10.1.2.3, tissue-equivalent proportional counters (TEPCs) are capable of measuring absorbed dose to the sensitive gas volume and of determining an approximation of the dose equivalent by its spectroscopic properties. They thus provide additional information normally not available from other neutron-measuring instruments. Due to practical limitations, however, TEPCs are not yet readily usable in everyday routine monitoring [01ICR, 00Sha].

For *personal monitoring* in mixed n-γ fields, the most commonly used devices today are albedo TLD badges, containing TL detector chips with a high fraction of ^{6}LiF (such as TLD-600), that has a large ^{6}Li (n,α) ^{3}H cross section for thermal neutrons, as well as chips with a high fraction of ^{7}LiF (such as TLD-700), that is insensitive to neutrons. The dosimetry of fast neutrons becomes possible when the batch is held closely to the body where it will be exposed to low energy neutrons that are backscattered from the body as the result of the moderation of fast neutrons within the body. These scattered neutrons are called albedo neutrons. As an example, Fig. 10.21 shows the schematic design of a TLD albedo dosimeter that consists of two pairs of ^{6}LiF - ^{7}LiF detectors. One pair is shielded from the rear with a thermal-neutron absorber (e.g. cadmium- or boron-loaded plastic) the second from the front. The readings obtained from the incident-neutron and albedo-neutron detectors are combined into an overall calculation of neutron dose equivalent. It should be mentioned, however that the resulting dose equivalent response of the dosimeter varies greatly with neutron energy at intermediate and high energies. Therefore, a single calibration factor cannot be used in different neutron fields with widely varying spectra if accurate dose results are to be obtained. In such cases, it is necessary to keep a record of the location in which the TLD batch was used, and to apply the appropriate calibration factor for the reading [01ICR].

Alternatively, etched-track detectors are used for neutron personal dosimetry. These passive devices utilize the ability of some materials to register the tracks of (neutron induced) charged particles as damage to their structure. The permanent damage tracks can be greatly enlarged by chemical or electrochemical etching procedures. The resulting conical etched pits in the material at the damage sites are visible to the naked eye and can be counted automatically by optical systems. Most frequently, plastic foils of 'polyallyl diglycol carbonate' (PADC, also known by the trade name CR-39) are used, which are uniquely sensitive to recoil protons released by neutrons passing through the material. PADC is sensitive to fast neutrons with an energy down to about 100 keV, and, by adding a converter layer, also to thermal and epithermal neutrons. PADS foils are insensitive to photons and β-particles and are thus suitable to measure the neutron component in a mixed n-γ field [01ICR, 97Bar]. (Due to the same reason, PADC detectors are used to estimate personal radon doses as well as integrated indoor radon concentrations by detecting the α-particles from the decays of radon and its daughter products.)

Superheated-drop or bubble detectors can be employed for both area and personal monitoring. They consist of microscopic droplets of liquid halocarbons and hydrocarbons dispersed in a gel or polymer matrix. The liquid droplets are superheated and are thus in a metastable state. When a neutron interacts with a nucleus inside or near a droplet, the resulting secondary charged particles locally increase the temperature and thus cause local vaporization. By this process, small vapor bubbles are formed that begin to expand by vaporizing adjoining liquid. If a vapor bubble reaches a critical size, all of the liquid in the droplet will be vaporized resulting in a visible gas bubble with a diameter of up to a millimeter. If the neutron energy exceeds a specific detector threshold – which depends on the atomic composition and size of the superheated droplets and the temperature and pressure of the matrix – the overall absorbed energy is correlated to the number of bubbles in a vial [01ICR, 00Kno, 00Sha]. Typical sensitivities are in the range of a few bubbles per μSv. Bubble detectors can be constructed as passive or active devices. In the first case, the superheated droplets are dispersed in a viscous polymer gel so that the bubbles remain fixed and thus can be counted at the end of the measurement by eye or automatically using an optical scanner. Active devices can be realized, for example, by placing an electro-acoustic transducer in contact with the detector, so that each time a bubble is formed, the sound that is produced is converted into an electrical pulse. An important feature of all superheated drop detectors is their almost complete insensitivity to photons and electrons with energies up to about 6 MeV [01ICR].

Further types of neutron detectors for area and personal monitoring as well as guidance concerning the measurement of operational dose equivalent quantities for neutron radiation are given in [01ICR, 99Alb].

10.1.8 Biological dosimetry

The human genome contained in the cell nucleus is physically carried by 46 chromosomes, each of which is composed of an extremely long, double-stranded helical DNA molecule in a closely packed form. Chromosomes are clearly visible through a light microscope during the metaphase – a certain stage of cell division, in which the condensed chromosomes become attached to spindle fibers and lie in a central plane of the nucleus. In this stage of cell cycle, chromosomes are already replicated (doubled). The newly formed twin chromosomes, which are called chromatides, remain temporarily attached to each other at a point, the centromere, located near the center of each of the chromatides (Fig. 10.22a).

There is a large body of evidence that biological effects of ionizing radiation result principally from damage to DNA. The most important effects caused by ionizing radiation are breaks in the DNA double helix. Single-strand breaks are restored immediately by molecular repair mechanisms using the opposite DNA strand as a template. If the repair is incorrect, the genetic information is altered. Although such point mutations may lead to inherited effects of offspring or the induction of carcinogenesis, they do not result in chromosomal aberrations visible under the microscope. On the other hand, breaks at both strands on opposite sides of the double helix that are juxtaposed may lead to a double-strand break. When this happens, different types of chromosomal aberrations can be observed: If the radiation-induced damage occurs before the chromosomes have been replicated, the lesion is dublicated during DNA synthesis and thus both chromatides show the same aberration (chromosome aberration). If, on the other hand, the cell

is irradiated after the DNA material has already been doubled, only one of the two twin chromatides is damaged (chromatide aberration). Gross distortions that are clearly visible in the metaphase are di- and tricentric chromosomes. They are formed when a break occurs in two or even three chromosomes and the centric fragments – carrying the centromere – incorrectly join with each other at their broken ends. The remaining acentric fragments are lacking a centromere and can thus easily be detected in the metaphase, too. A detailed description of the various types of radiation-induced chromosomal aberrations is presented in [00Hal].

Cytogenetic analysis of chromosomal aberrations is a valuable tool for retrospective dose assessment of individuals that are accidentally overexposed to ionizing radiation. It fills a gap in dosimetry, since the radiation effect on the human body is determined directly without the intermediary of dosimetric measurements using technical devices. Scoring of chromosome aberrations in peripheral blood lymphocytes, mainly the dicentric assay, is regarded as the most specific method and has become a routine component of accidental dose assessment [02Voi]. Figure 10.22a shows representative chromosome aberrations in a metaphase preparation of irradiated lymphocytes. Many studies in animals and humans have shown a good relation between the results obtained *in vivo* and *in vitro* and this provides evidence that *in vitro* established dose-effect relationships can be used as calibration curves [02Voi]. However, as shown in Fig. 10.22b, the formation of dicentrics strongly depends on radiation quality and dose rate so that information about these variables needs to be established for each investigation. As mentioned above, DNA breaks must be induced in two different unreplicated chromosomes in order to form a dicentric chromosome. Since this can be achieved either by a single particle breaking on occasion both chromosomes or two particles each of which damaging only one chromosome, the frequency N of dicentric chromosomes per cell can be well fitted as a function of dose D by a linear-quadratic model, $N = \alpha D + \beta D^2$. At low doses, one-particle events (described by the linear term, αD) are more frequent, whereas two-particle events (described by the quadratic term, βD^2) dominate at high doses. Besides the calibration curve used, the precision of dose estimation depends mainly on the number of cells observed and the background level. In practice, detection of low LET radiation is possible for doses above 150 mGy [02Voi].

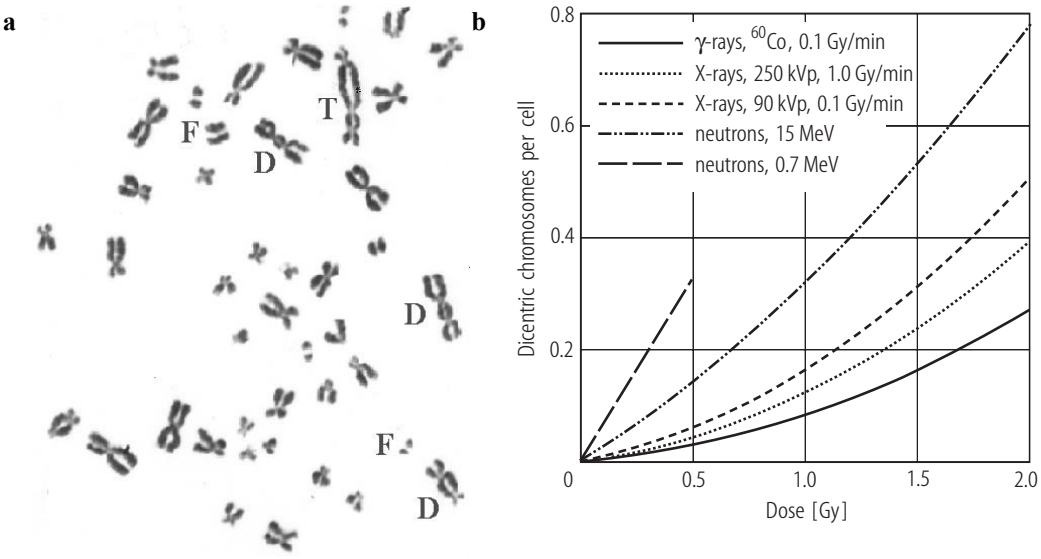

Fig. 10.22. Radiation-induced chromosomal aberrations in human lymphocytes. **(a)** Metaphase preparation with normal, dicentric (D), and tricentric chromosomes (T) as well as various fragments (F). **(b)** Frequency of dicentric chromosome aberrations per cell for several types of radiation. The curves give the result of linear (low-energy neutrons) and linear-quadratic fits to measured data. (Courtesy G. Stephan, BfS).

10.1.9 References for 10.1

68Att Attix, H., Roesch, W.C., Tochilin, E.: Radiation Dosimetry. 2nd edition, Vols. I-III. New York: Academic Press, 1968-1969.

72Kie Kiefer, H., Maushardt, R.: Radiation Protection Measurement. Oxford: Pergamon Press, 1972.

79ICR ICRU Report 31: Average energy required to produce an ion pair. Bethesda, MD: ICRU Publications, 1979.

81Bar Barrett, H.H., Swindell, W.: Radiological Imaging. London: Academic Press, 1981.

83ICR ICRU Report 36: Microdosimetry. Bethesda, MD: ICRU Publications, 1983.

86Att Attix, F.H.: Introduction to radiological physics and radiation dosimetry. New York: John Wiley & Sons Inc., 1986.

86Sch Scharmann, A, Kriegseis, W.: Radiat. Prot. Dosim. **17** (1986) 359.

87Per Perry, J.A.: RPL Dosimetry: Radiophotoluminescence in health physics. Bristol: IOP Publishing, 1987.

89Die Dietze, G., Menzel, H.G., Schuhmacher, H.: Radiat. Prot. Dosim. **28** (1989) 77.

89Men Menzel, H.G., Paretzke, H.G., Booz, J. (eds.): Implementation of dose-equivalent meters based on microdosimetric techniques in radiation protection; Radiat. Prot. Dosim. **29** (1-2) (1989).

93Pie Piesch, E., Burgkhardt, B., Vilgis, M.: Radiat. Prot. Dosim. **47** (1993) 409.

94ICR1 ICRU Report 52: Particle counting in radioactivity measurements. Bethesda, MD: ICRU Publications, 1994.

94ICR2 ICRU Report 53: Gamma-ray spectrometry in the environment. Bethesda, MD: ICRU Publications, 1994.

94Leo Leo, W.R.: Techniques for nuclear and particle physics experiments, 2nd edition. Berlin: Springer-Verlag, 1994.

95Hir Hirning, C.R.; Yuen, P.S.: Health Phys. **69** (1995) 46.

95ISO International Organization for Standardization: Guide to the expression of uncertainty in measurement. Geneva, Switzerland: ISO, 1995 (corrected of first print in 1993).

95Sch Schmitz, Th., Waker, A.J., Kliauga, P., Zoetelief, H. (eds.): Design, construction and use of tissue-equivalent proportional counters – EURADOS report; Radiat. Prot. Dosim. **61** (4) (1995)

95Tso Tsoulfanidis, N.: Measurement and detection of radiation, 2nd edition. Washington: Taylor & Francis, 1995.

95Wak Waker, A.J.: Radiat. Prot. Dosim. **61** (1995) 297.

96Hoh Hohlfeld. K.: Nachweismethoden für ionisierende Strahlung, in: Kose, V.; Wagner, S. (eds.), Praktische Physik, Band 2. Stuttgart: B.G. Teubner, 1996, Kapitel 7.4.

96Kah Kahilainen, J.: Radiat. Prot. Dosim. **66** (1996) 459.

96Ols Olsher, R.H., Eisen, Y.: Radiat. Prot. Dosim. **67** (1996) 271.

97Bar Bartlett, D.T.; Steele, J.D., Tanner, R.J., Gilvin, P.J., Shaw, P.V., Lavelle, J.: Radiat. Prot. Dosim. **70** (1997) 161.

99Alb Alberts, W.G., Arend, E., Barelaud, B., Curzio, G., Decossas, J.L., d´Èrrico, F., Fiechtner, A., Grillmaier, R., Meulders, J.-P., Menard, S., Roos, H., Schuhmacher, H., Thevenin, J.-C., Wernli, C., Wimmer, S.: Advanced methods of active neutron dosimetry for individual monitoring and radiation field analysis (ANDO), Report PTB-N-39, Braunschweig, 1999.

99Lut Lutz, G.: Semiconductor radiation detectors. Device Physics. Berlin: Springer-Verlag, 1999.

99Sak Sakurai, T.; Tomita, A., Fukuda, Y.: J. Phys. D **32** (1999) 2290.

99Wer Wernli, C., Fiechtner, A., Kahilainen, J.: Radiat. Prot. Dosim. **84** (1999) 331.

00Hal Hall, E.J.: Radiobiology for the radiologist, 5th edition. Philadelphia: Lippincott Williams & Wilkins, 2000.

00Kno Knoll, G.F.: Radiation detection and measurement, 3rd edition. New York: John Wiley & Sons, Inc. 2000.

00Sha Shani, G.: Radiation dosimetry: Instrumentation and methods, 2nd edition. Boca Raton: CRC Press 2000.

01ICR ICRU Report 66: Determination of operational dose equivalent quantities for neutrons. Journal of the ICRU, Volume 1, No 3, 2001.
01Tak Takahashi, T; Watanabe, S.: IEEE Trans. Nucl. Sci. **48** (2001) 950.
02Bus Bushberg, J.T.; Seibert, J.A., Leidholdt, E.M., Boone, J.M.: The Essential Physics of Medical Imaging, 2nd edition. Philadelphia: Lippincott Williams & Wilkins, 2002,.
02ISO ISO/ASTM51707-2002(E): Guide for estimating uncertainties in dosimetry for radiation processing. Geneva, Switzerland: International Organisation for Standardization, 2002.
02Sai Saint-Gobain Crystals & Detectors: Product Data Sheets, www.detectors.saint-gobain.com.
02Voi Voisin, P.; Barquinero, F., Blakely, B., Lindholm, C., Lloyd, D., Luccioni, C., Miller, S., Pallitti, F., Prasanna, P.G., Stephan, G., Thierens, H., Turai, I., Wilkinson, D., Wojcik, A.: Cell. Mol. Biol. **48** (2002) 501.
02Wak Waker, A.J.; Schrewe, U., Burmeister, J., Dubeau, J., Surette, R.A.: Radiat. Prot. Dosim. **99** (2002) 311.